

First Evaluations of Airborne InSAR Time-Series

Karlus A. C. de Macedo*, Rolf Scheiber, Alberto Moreira
Microwaves and Radar Institute (DLR), Germany

*The author holds a Grant from CAPES, Brazil

Abstract

To allow time-series analysis of airborne SAR images using PSs (Permanent Scatterers), this paper has two main objectives. The first is to show, in a quantitative way, that there is a compromise between the number of images used to detect PSs, their probability of being detected and their stability. This tradeoff is derived based on estimation and detection theories. The second objective is to investigate the possibility of the use of permanent scatterers to estimate undesired phase undulations in airborne data due to residual motion errors. A new technique is proposed, the so-called PS-PGA, where we apply the Phase Gradient algorithm on the PSs in order to obtain sub-wavelength estimations of residual motion errors for both master and slaves, separately, differently from current approaches. Compensation of these residual errors will lead to more reliable airborne D-InSAR measurements.

1 Introduction

In order to compensate in interferograms undesired phase contributions due to atmospheric effects, DEM errors, [1] proposes the Permanent Scatterer technique (PS). The PS technique involves the selection of phase-stable scatterers, Atmospheric Phase Screen (APS) estimation and compensation, parameter inversion of terrain deformation, and DEM errors from a series of SAR data. This technique has been successfully applied to spaceborne data where sets of more than 30 images are oft available. For reliable APS estimation using the PS technique, [2] shows that more than 20 images are necessary. In this paper we investigate for the first time the use of the PS technique in airborne data. Differently from spaceborne case, atmospheric effects are not the main source of undesired phase contribution in airborne data. For the airborne case the accuracy of the phase measurements are mainly affected by the deviations of the platform from the nominal track. After very precise motion compensation [3], residual motion errors in the order of 5-10 cm are still present in the image causing significant phase undulations turning D-InSAR applications (sub-wavelength measurements) with airborne data impracticable.

Due to the low availability of large sets of data from airborne platforms, we start our investigation with a set of 14 images of the E-SAR system acquired in the same day. Due to the different nature of phase errors between spaceborne and airborne case, it may be possible, differently from APS estimation, to use less than 20 images to estimate residual motion errors, as we will show. To have a robust and reliable selection of PSs with 14 SAR images we developed and propose a quantitative analysis of the permanent scatterers selection performance.

It is shown in [1] and [4] that, the more images available the smaller is the estimation error of the dispersion index estimates \hat{D}_A . But up to now, there is no quantitative relation showing the tradeoff between the number of images, the desired phase stability and detectibility of the selected permanent scatterers.

In section 2, we derive a tradeoff relationship of the compromise between the number of images to detect PS candidates, their stability, and their probability of detection. In section 3, we use the selected PSs to estimate undesired phase undulations in airborne data due to residual motion errors. We propose a new technique, the so-called PS-PGA, where we apply the Phase Gradient algorithm on the PSs in order to obtain sub-wavelength estimations of motion error. A discussion of the results is included in Section 4.

2 The PS Selection Performance

2.1 Stability

The PS technique identifies the stable-phase or permanent scatterers by performing a statistical analysis of the amplitude values of a scatterer along a series of SAR acquisitions. From the amplitude dispersion index D_A , it is possible to estimate the phase standard deviation σ_ν of a scatterer [1]

$$\sigma_\nu \simeq \frac{\sigma_n}{g} \simeq \frac{\sigma_A}{m_A} \triangleq D_A, \quad (1)$$

where g and σ_n are the parameters of the Rice PDF (Probability Density Function) which models the amplitude of the radar scatterers [1], and m_A and σ_A are the mean and the standard deviation of the amplitude values of the scatterer, respectively. The selected permanent scatterers are those in which the amplitude dispersion, D_A , is lower than a certain threshold value. Alternatively to D_A , the stability of a scatterer can be given by its SNR (Signal to Noise Ratio). It is found by dividing the mean power P of the signal of the scatterer by the power of the noise N_o , i.e. P/N_o . For a scatterer with Rice distributed amplitudes it becomes

$$SNR = \frac{P}{N_o} = \frac{g^2}{2\sigma_n^2}. \quad (2)$$

Note, through (2) and (1), that the SNR and the dispersion index are coupled, i.e.

$$D_A \simeq \frac{1}{\sqrt{2SNR}}. \quad (3)$$

Thus, a scatterer is defined as a PS if its dispersion D_A is lower than a certain threshold value. We will call this value as the dispersion index of a PS, D_{PS} . The D_{PS} is an arbitrary value which corresponds to the desired phase stability of a scatterer. Different criterias of phase stability or of what is a PS or not, can be set by redefining D_{PS} . The desired stability of a PS depends on the accuracy and application demands.

The permanent scatterers in a SAR image can be selected (detected) by thresholding the values of the dispersion index D_A through a dispersion threshold D_T . Defining a D_T implies in a probability of detecting a PS (P_d) or selecting a scatterer that is not a PS (P_{fa}).

At this point, it is important to make a distinction between D_{PS} and D_T . Although they can have the same value, they are not necessarily equal since D_{PS} is the value of dispersion used to define what is a PS and what is not, while D_T is the value which we set in order to minimize the false alarm rate or maximize the probability of detection of PS as it will be detailed in the next subsection.

2.2 Detection and False Alarm Rate

Let the hypotheses be: H_0 there is no PS, i.e. the scatterer (with Rice distributed amplitude) has a dispersion greater than D_{PS} , or H_1 there is a PS, i.e. the scatterer (with Rice distributed amplitude) has a dispersion less or equal than D_{PS} . Let the PDF of the estimates \hat{D}_A of the dispersion index be given by $f_{\hat{D}}(\hat{d})$. According to detection theory [5], we have for the discrete random variable case

$$P_d = \sum_{i=0}^{D_T} f_{\hat{D}}(\hat{d}_i | H = H_1) \delta(\hat{d} - \hat{d}_i), \quad (4)$$

$$P_{fa} = \sum_{i=0}^{D_T} f_{\hat{D}}(\hat{d}_i | H = H_0) \delta(\hat{d} - \hat{d}_i), \quad (5)$$

where P_d is the probability of detection, P_{fa} is the probability of false alarm of a PS, and $\delta(\hat{d})$ is a Dirac function.

In a simulation, the PDF $f_{\hat{D}}(\hat{d})$ is obtained numerically [5], building the histograms of M estimates of \hat{D}_A for a given number N of images. The true value of SNR and D_A are known in the simulation and coupled through (3). While the true D_A value is less or equal than D_{PS} , the hypothesis H_1 is valid and (4) is used to compute the P_d . When the true D_A reaches a value greater than D_{PS} , the hypothesis H_0 is made valid and (5) is used to compute P_{fa} . **Figure 1** shows $f_{\hat{D}}(\hat{d})$ for H_0 and H_1 with $M=5000$, $N=34$, $D_{PS}=0.25$ and $D_T=0.20$. **Figure 1a** corresponds to the hypothesis H_1 (there is a PS). The probability of detection is given by the area below the curve of $f_{\hat{D}}(\hat{d})$ in the interval $[0, D_T]$. **Figure 1b** corresponds to the hypothesis H_0 (there is no PS). The false alarm rate is given by the area below the curve $f_{\hat{D}}(\hat{d})$ in the interval $[0, D_T]$.

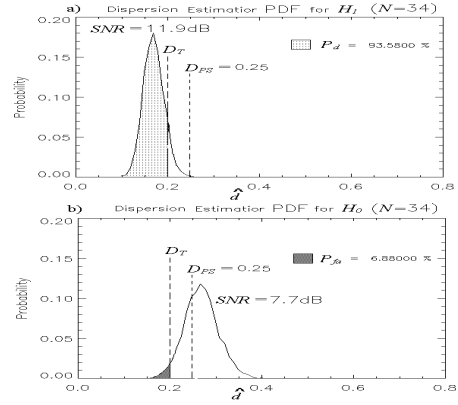


Figure 1: Histogram of $f_{\hat{D}}(\hat{d})$ showing the P_d and P_{fa} of 2 different scatterers, (a) a PS and (b) not a PS.

2.3 Selection Performance

We can now analyse the performance of the permanent scatterers selection in terms of stability (the defined D_{PS}) and detectability (P_d and P_{fa}), for different SNR's (100 different values of SNR between -3.4 to 23dB were used). **Figure 2a** shows the probability of detection for a fixed threshold and varying the number of images used. We see that the greater the number of images more abrupt is the variation of the probability of detection as a function of the SNR. This means that, when the number of images increases, a very accurate selection is performed and almost every PS is detected. **Figure 2b** shows the false alarm rate for a fixed threshold $D_T=0.2$ and varying the number of images used. We see that the greater the number of images, the lower is the peak of the false alarm rate as well as the area below the curve. This means that, when the number of images increases, less scatterers are being mistaken and the ones wrong selected are very close to be a PS.

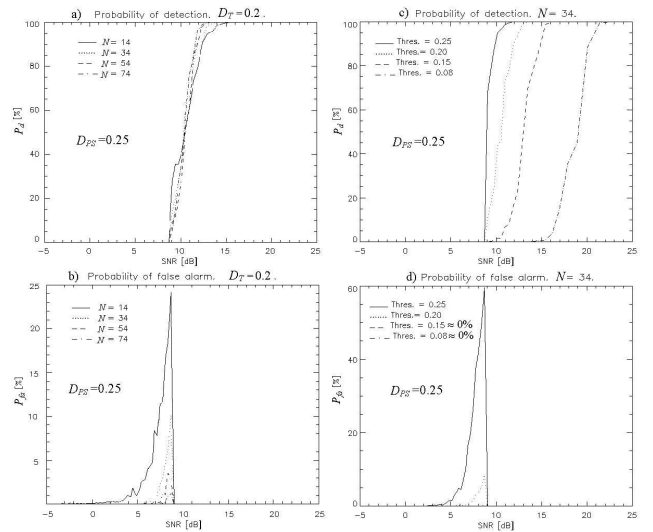


Figure 2: Probability of detection (a) and false alarm (b) of PS ($D_{PS}=0.25$) for a fixed threshold $D_T=0.20$ and varying the number of images used. Idem in (c) and (d) for a fixed number of images $N=34$ and varying D_T .

Figure 2c shows the probability of detection for a fixed number of images and varying the threshold D_T . We see that by decreasing the Dispersion threshold the curve of P_d moves towards increasing SNR values, which means that only scatterers with high SNR have 100% of chance to be selected as PS. Consequently, when the threshold decreases, the number of detected PS decreases. **Figure 2d** shows the probability of false alarm for a fixed number of images and varying the threshold D_T . We see that by decreasing the Dispersion threshold the peak of the curve of P_{fa} decreases as well as the area below the curve (similar to **Figure 2b**). This means that, for lower thresholds we have lower false alarm rates.

We can conclude now that varying the threshold D_T we can control the probability of detection and false alarm of PS. The lower the threshold, the lower is the probability of detection as well as the false alarm. The higher the threshold, the higher is the probability of detection as well as the false alarm. The desired performance is a high probability of detection and a low false alarm rate. A compromise between number of images, detection and false alarm rate has to be found.

Since the P_d and P_{fa} vary with the SNR, in a typical SAR image we have different P_d and P_{fa} for different scatterers. To have a reference value of the performance of detectability, we define \bar{P}_d and \bar{P}_{fa} as being the average probability of detection and maximum false alarm of PSs, respectively. The \bar{P}_d is here defined as the average of the function P_d vs. SNR. It is taken in the interval $[SNR_{PS}, SNR_{PT}]$, where SNR_{PS} is obtained substituting D_{PS} in (3), and where SNR_{PT} is the dispersion index of a point-like target. The point-like target is a reference value. In our case, 2m resolution image (E-SAR system), SNR_{PT} is 23dB, estimated from isolated corner reflectors located in the image. For Q samples of SNR we have

$$\bar{P}_d \triangleq \frac{1}{Q} \sum_{q=0}^{Q-1} P_d(SNR_q), \quad (6)$$

where $SNR_0 = SNR_{PS}$ and $SNR_{Q-1} = SNR_{PT}$. The \bar{P}_{fa} is defined as the maximum probability of false alarm in the function P_{fa} vs. SNR. This means that for every possible SNR in the SAR image the possibility of mistaking a scatterer as a PS is equal or less than

$$\bar{P}_{fa} \triangleq \max\{P_{fa}\}. \quad (7)$$

Table 1 shows the performance of the selection of PSs ($D_{PS}=0.25$) in terms of \bar{P}_d , \bar{P}_{fa} , for different number of images and thresholds.

N [images]	D_T	\bar{P}_d	\bar{P}_{fa}
14	0.06	17%	$\leq 10^{-3}\%$
14	0.08	24%	$10^{-2}\%$
14	0.20	80%	24%
34	0.20	81%	10%
84	0.20	81%	1%

Table 1: Some PS ($D_{PS}=0.25$) selection performance

2.4 The selected PSs on Real Data

The data set used for the first time-series analysis is composed of 14 images (L-Band) acquired in the same day (May 11, 1998) and perpendicular baselines going from -105 to 108 meters. For a reliable selection of PSs, **Figure 3**, the \bar{P}_{fa} has to be less or equal $10^{-3}\%$. This conclusion comes from the fact that taking a window of 100x100 pixels over homogenous areas like grass we have around 30 selected PSs random distributed inside. This is 0.3% of the total number of scatterers. Analysing the amplitude value in the window, no prominent peak was found and the SNR is low, which makes us conclude that PS selection with $\bar{P}_{fa} = 3\%$ is not robust in vegetated areas. Thus, for 14 images the selection of PS ($D_{PS} = 0.25$), over vegetated area, is possible only by setting $D_T=0.06$ in order to have $\bar{P}_{fa} \leq 10^{-3}\%$ but paying the price of having only $\bar{P}_D = 17\%$. This performance can be seen in **Figure 3**. To verify this we analyse the scatterers belonging to a fence at the right of the runway. This fence has high SNR and has a lot of PSs with $D_{PS} \leq 0.25$. We see that for around 800 pixels belonging to the fence, we only have about 50 (7%) that are being detected as PS with $D_T = 0.06$. Another indication of the low detectability are the 9 corner reflectors located in the image and marked with white circles. Four out of nine corners are selected as PS.

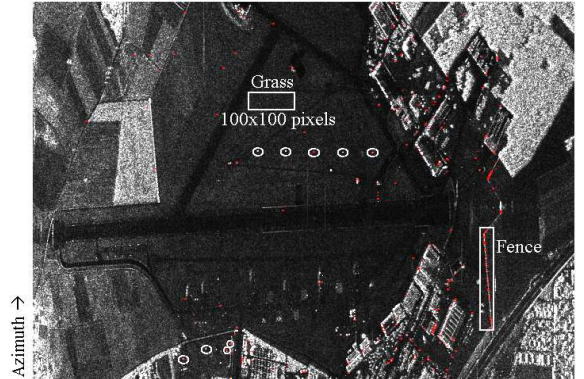


Figure 3: Selected PSs (in red) with $D_T = 0.06$.

3 The PS-PGA Technique

The PGA (Phase Gradient Autofocus) implements the MVU (Minimum Variance Unbiased) estimator of the phase error gradient of a SAR image [6]. The PGA models the complex SAR scatterer as being a deterministic scatterer in White Gaussian Noise (WGN). As long this model is valid the PGA will lead to the MVU estimation. The idea of the here proposed PS-PGA technique is to exploit the fact that we are able to find PSs, which are the scatterers that fit very consistently into this model, especially if this PS is isolated in a small window of the image. We introduce then the IPS (Isolated PS) scatterers concept. We can find IPSs defining two possible criteria. A PS is a IPS if the SNR between the main and second lobe of the SAR IRF (Impulse Response Function) inside the

window is greater than a certain threshold SNR_T . We use as SNR_T the value that corresponds to $D_{PS}=0.25$ using (3). For the moment we use a 25×25 window. The second criteria is to verify if the 3dB value of the amplitude of the PS is equal or less the theoretical resolution of the image. Using these criteria we can be sure that there is only one principal scatterer inside the window. About 50% of the selected PSs turned out to be IPSs.

The PS-PGA algorithm is implemented for strip-map focused images by taking each of the IPSs inside their corresponding window, decompressing the IPS, and deramping it to obtain $g_k(t)$ [7]. Then we apply the phase gradient estimator

$$\hat{\phi}_e = \frac{\sum_{k=1}^K \text{Im}[g_k(t)g_k^*(t)]}{\sum_{k=1}^K |g_k(t)|^2}, \quad (8)$$

where k is the index for K IPSs that have overlapping apertures. Using (8), the phase gradient estimation phase estimation is non range-dependent. For a first preliminary analysis of the results this is not a problem.

The PS-PGA technique is intended to be used for estimation of residual motion errors of airborne SAR systems. After precise topography- and aperture-dependent Motion Compensation, PTA-MoComp [3], residual motion errors (in the order of 5 to 10cm) are still present due to DEM and navigation system inaccuracies causing phase errors in the final interferogram. These residual phase errors turns D-INSAR measurements impractical. Working with PSs, our estimation with PGA will be very robust and accurate leading to a phase estimation, after integrating (8), that can reach sub-wavelength accuracy. That is the main difference to conventional PGA. In the latter case the selection of points to be used in the estimation is based only on the brightness of the target, which can lead to inaccurate estimations when most of the targets chosen do not fit the assumed model (strong target in WGN).

Note that PS-PGA requires InSAR steps. To identify the PSs the images have to be already well focused and to sub-pixel level coregistered. Thus PS-PGA is not intended for defocused images, but to estimate phase errors at PS-scale, i.e., sub-pixel scale [1], improving interferometric accuracy.

Figure 4 shows the PS-PGA phase error estimation (mid-range) for the master image and one of the slaves from the 14 images data set. As each PS gives an estimate for a whole synthetic aperture, a very high density of PSs is not necessary. **Figure 4** also shows the intererometric phase error between them (up to 30 degrees in this case). Compensation of this phase error can be done using PTA-MoComp [3], independently for each image. Another technique for estimation of residual motion error for interferometric pairs is described in [8], but in this approach independent estimation for master and slave errors is not possible.

4 Conclusions

A selection performance analysis of PSs was derived. This statistical analysis is very important when accessing the quality and reliability of the selected PSs. In addition first results

of the here proposed PS-PGA technique look very promising and the range-dependent PGA estimator will be implemented in a next step. The acquisition of more interferograms will lead to more PSs and to a reduction of the estimation error. Since PS-PGA is meant for D-INSAR applications, a series of acquisition along time is not a constraint since after compensation of residual phase errors, this time series will be used to estimate parameters as terrain deformation velocities and DEM errors. Further work consists in evaluating the improvement of airborne D-InSAR measurements after compensating the residual motion errors estimated by PS-PGA and to access their accuracy as a function of the number of PSs.

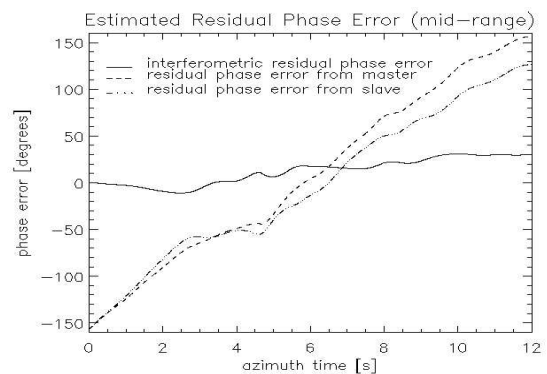


Figure 4: PS-PGA result for a interferometric pair.

References

- [1] A. Ferretti, C. Prati, F. Rocca: *Permanent Scatterers in SAR Interferometry*, IEEE Trans. Geosci. Remote Sensing, vol. 39, no. 1, pp. 8-20, Jan. 2001.
- [2] C. Colesanti, A. Ferretti, F. Novali, C. Prati, F. Rocca: *SAR Monitoring of Progressive and Seasonal Ground deformation using the Permanent Scatterer Technique*, IEEE Trans. Geosci. Remote Sensing, vol. 41, no. 7, pp. 1685-1701, Jul. 2003.
- [3] K.A.C. de Macedo, C. Andres, R. Scheiber: *On the Requirements of SAR Processing for Airborne Differential Interferometry*, Proc. IGARSS'05, Seoul, South Korea, Jul. 2005.
- [4] N. Adam, B. M. Kampes, M. Eineder: *The development of a scientific permanent scatterer system: Modification for mixed ERS/ENVISAT time series*, Proc. ERS & ENVISAT Symposium, Salzburg, Austria, Sept. 2004.
- [5] L. Scharf: *Statistical Signal Processing: Detection, Estimation and Time Series Analysis*, Addison-Wesley, New York, NY, 1990.
- [6] P.H. Eichel, C.V. Jakowatz, "Phase-gradient algorithm as an optimal estimator of the phase derivative", Optics letters, vol. 14, no. 20, pp.1101-1103, Oct. 1989.
- [7] D.E. Wahl, C.V. Jakowatz, P.A. Thompson, "New approach to strip-map SAR autofocus", Proc. VI IEEE Digital Signal Processing Workshop, pp.53-56, Josemita, California, Oct. 1994.
- [8] P. Prats, A. Reigber, J.J. Mallorqui: *Interpolation-Free Coregistration and Phase-Correction of Airborne SAR Interferograms*, IEEE Geosci. Remote Sensing Lett., vol. 1, no. 3, pp.188-191, Jul. 2004.